One-dimensional transport-induced instabilities in an optical system with nonlocal feedback

P. L. Ramazza, P. Bigazzi, E. Pampaloni, S. Residori, and F. T. Arecchi
Istituto Nazionale di Ottica, Largo Enrico Fermi 6, 50125 Firenze, Italy
(Received 23 May 1995)

We present theoretical and experimental evidence of pattern forming instabilities induced by the non-local interaction of the light signal with itself, in an optical system formed by a liquid-crystal light valve with feedback. For a defocusing medium, the model predicts a reduced instability threshold for pattern formation as a result of nonlocality. The conditions for the onset of drifting mode instability are analytically derived. The experimental results quantitatively confirm the predictions of the model.

I. INTRODUCTION

In recent years the physics of pattern formation in systems far from thermodynamical equilibrium has attracted increasing attention [1]. In this context, hydrodnamical and chemical systems were studied first. It was later recognized that the field of nonlinear optics also offers a rich variety of systems giving rise to structure formation and competition phenomena [2]. In fact, nonlinear optical systems can encompass most of the mechanisms (e.g., nonlinearities, role of boundary conditions, diffusion) that were previously recognized to be at the basis of pattern formation in systems of other kinds. The wave nature of the optical fields was then shown to be at the basis of an interesting class of pattern forming instabilities [3].

In this paper we report the theoretical and experimental investigation of the instabilities that arise in a one-dimensional system formed by a liquid-crystal light valve (LCLV) with feedback, when a translation is introduced in the feedback loop of the device. The translation induces a nonlocal interaction of the signal with itself. Similar kinds of interaction, introduced in the same system either via a magnification or via a rotation of the feedback field, have proved to be efficient in destabilizing the uniform state of the signal, and to force the symmetries of the nascent pattern [4,5]. The one-dimensional transport term, here introduced in the material equation by the translation, is similar to that previously introduced to account for a tilt of the incoming wave in the case of a Fabry-Perot resonator filled with a nonlinear medium [6,7], or of an optically nonlinear slice with a feedback mirror [8,9]. As in these two cases, the main effect generated by the transport term is the destabilization of the uniform solution for the signal, in favor of traveling wave solutions (drift instability).

Drifting patterns were previously reported as stemming from primary bifurcations in Rayleigh-Benard convection in a binary mixture [10], in the flow between two cylinders with a partially filled gap [11], and in electroconvection in nematics [12]. Drifting patterns stemming from secondary bifurcations, i.e., from destabilization of a stationary nonuniform solution, were observed in a Faraday instability experiment [13] and in directional viscous fingering [14]. For this second kind of bifurcation a general model based on symmetry breaking arguments has been developed [15]. Although the situations listed above cannot be reduced to a uniform model, we notice that in many of these experiments nonlocal interaction between the dynamical variables comes into play. This suggests that the role of nonlocality in inducing drifting patterns may be rather general.

Returning to optics, the main advantages of our setup, as compared to the previous ones, lies in the fact that the LCLV device providing the nonlinearity works at low input intensities (typically some mW/cm^2) an has a response time of the order of 100 ms. Hence it is possible on one side to resolve the spatiotemporal dynamics of the signal, and on the other to scan the control parameter (input intensity) over a wide range from very close to threshold to far away from it, thus displaying some phenomenologies that are unexpected on the basis of the linear stability analysis.

II. EXPERIMENTAL SETUP

The experimental setup is shown in Fig. 1. A beam from an Ar^+ laser operating at 514 nm is expanded and collimated by means of the lenses L_0 and L_1, and then sent on the front face of the LCLV. This device operates in reflection, inducing a phase retardation on the reflected beam that in a first approximation is a linear decreasing function of the light intensity illuminating the LCLV on the rear side [16]. In these operating conditions the LCLV is equivalent to a defocussing Kerr-like medium, with the characteristic controlled by the amplitude and frequency of the ac voltage applied to the device.

The reflected beam reaches plane z_i after a beam splitter (BS) and a mirror (M) passing through lenses L_1 and L_2. These two lenses are placed in a confocal configuration, so that the plane z_i is an (inverted) image of the plane containing the front face of the LCLV. In the plane z_i we put a 9.9×0.18-mm slit as a limiting aperture in order to build an almost one-dimensional constraint. In the following we call the long side of the slit the x direction. Starting from plane z_i the light beam undergoes free propagation over a length l, until it reaches one end of a fiber bundle. The fiber bundle coherently trans-
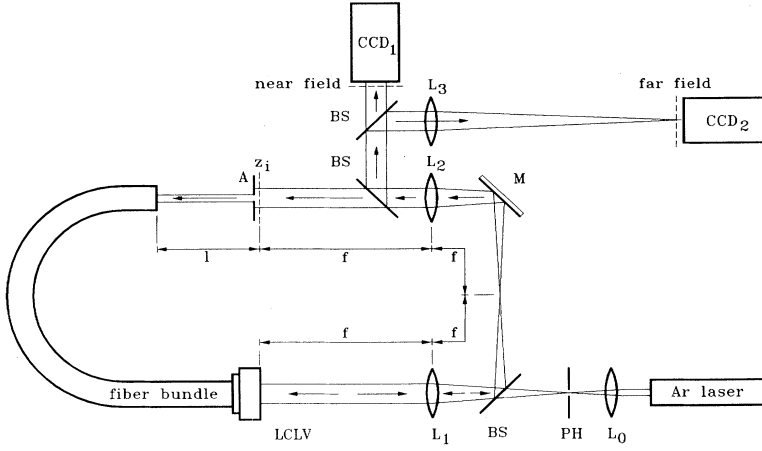
FIG. 1. Experimental setup. LCLV: Liquid crystal light valve; L_0, L_1, L_2, and L_3: lenses; BS: beam spliters; PH: pinhole; A: slit-like aperture; CCD1 and CCD2: video cameras.

ports the light from its entry to its exit face, that is optically connected to the rear face of the LCLV. A rotation of π of the fiber bundle across its axis provides compensation for the inversion of the image due to lenses L_1 and L_2. A translation of one of the ends of the fiber bundle along the x direction introduces a nonlocal interaction of the light beam with itself.

III. MODEL OF THE LCLV WITH TRANSLATED FEEDBACK

A light beam impinging on the front face of the LCLV as a plane wave of amplitude E_0 acquires, after reflection, a phase retardation $\varphi(x,t) = 2k_0 dn(x,t)$, where k_0 is the optical wave number, d is the thickness of the liquid-crystal layer, and $n(x,t)$ is the perturbation to the average index of refraction of the liquid crystals. For simplicity of notation, in the following we will identify the variables $\varphi(x,t)$ and $n(x,t)$. The reflected field at the exit of the LCLV thus has the form

$$E_{\text{out}}(z=0) = E_0 e^{in(x,t)} . \qquad (1)$$

This same field is present at plane z_i, where the slit is located. Let us consider a generical Fourier component of $n(x,t)$ at spatial frequency q:

$$n(x,t) = n_q(t)e^{iqx} + n_q^*(t)e^{-iqx} . \qquad (2)$$

Substituting this expression in (1) and assuming $n_q \ll 1$, we obtain

$$E_{\text{out}}(z=0) = E_0[1 + n_q(t)e^{iqx} + n_q^*(t)e^{-iqx}] . \qquad (3)$$

Due to free propagation from plane z_i to the entrance of the fiber bundle, the qth Fourier component of the field undergoes a phase shift $q^2l/2k_0$. It follows that, to first order in n, the intensity distribution reaching the fiber bundle is of the form

$$|E(z=l)|^2 = |E_0|^2 + 2|E_0|^2 \sin\frac{q^2l}{2k_0}[n_q(t)e^{iqx}$$
$$+ n_q^*(t)e^{-iqx}] . \qquad (4)$$

Let us now consider the equation governing the evolution

of the index perturbations in the liquid-crystal layer [4]:

$$\frac{\partial n(x,t)}{\partial t} = -\frac{n(x,t)}{\tau} + \frac{\partial^2 n(x,t)}{\partial x^2} + \alpha I_w , \qquad (5)$$

where τ is the local relaxation time, D the diffusion constant, and I_w the writing intensity impinging on the rear side of the LCLV. In the present case I_w is given by expression (4), in which we introduce the translation $x \to x + \Delta x$. Substituting this expression into (5) and specializing for the q Fourier component, it follows that

$$\frac{dn_q}{dt} = -\frac{n_q}{\tau} - Dq^2 n_q + 2\alpha|E_0|^2 \sin\frac{q^2l}{2k_0} n_q e^{iq\Delta x} \qquad (6)$$

plus the complex conjugate equation.

We now look for solutions of (6) of the form

$$n_q(t) = [\text{Re}(n_q(t)) + i\,\text{Im}(n_q(t))]e^{(\lambda + i\Omega)t} . \qquad (7)$$

Substituting in (6) and separating the real and imaginary parts of the resulting expression, we obtain

$$\lambda = -\frac{1}{\tau} - Dq^2 + 2\alpha|E_0|^2 \sin\frac{q^2l}{2k_0}\cos(q\Delta x) , \qquad (8a)$$

$$\Omega = 2\alpha|E_0|^2 \sin\frac{q^2l}{2}k_0\sin(q\Delta x) . \qquad (8b)$$

Equation (8a) gives the growth rate of a perturbation in the index of refraction at spatial frequency q. The condition $\lambda = 0$ gives the instability threshold for this Fourier component. Equation (8b) gives the temporal frequency at which the harmonic component at spatial frequency q oscillates. Recalling Eq. (2) for the form of $n(x,t)$ it is clear that the onset of an instability at a given q with $\lambda, \Omega \neq 0$ will result in the appearance of a roll-like pattern, drifting with a velocity $v_d = \Omega/q$. We observe that expressions (8) are analogous to those obtained in Ref. [8]. Following Ref. [3], we find it convenient to rewrite expressions (8) in a slightly different form, by introducing the quantities $l_d \equiv \sqrt{D\tau}$ (diffusion length of the liquid-crystal excitations), $\theta \equiv q^2l/2k_0$ (reduced wave number), $\sigma \equiv l/l_d^2 k_0$, $I_0 = |E_0|^2$, and $\beta \equiv 2\alpha\tau$. Then Eq. (8) reads

$$\tau\lambda = -1 - 2\frac{\theta}{\sigma} + \beta I_0 \sin\theta \cos(q\Delta x) \ , \tag{9a}$$

$$\tau\Omega = \beta I_0 \sin\theta \sin(q\Delta x) \ . \tag{9b}$$

IV. NUMERICAL RESULTS

In the present section we consider the quantities β, I_0, σ, and l as parameters, and study the behavior of the quantities $\tau\lambda$ and $\tau\Omega$ in the space of the variables $(\theta, \Delta x)$ (we notice that q can be obtained from θ if l is known). The right-hand side of Eq. (9a), giving the growth rate of

a perturbation of index of refraction with the reduced wave number θ, is a superposition of a plane of negative slope $2/\sigma$ along θ, plus a term that has a harmonic dependence both along θ and Δx. The first term represents the contribution of local relaxation and diffusion to the decay of perturbations. The larger the diffusion length, the smaller σ is, and this contributes to lower the growth rate for the modes at high θ. The second term comes from the Kerr nonlinearity of the LCLV, and its magnitude and sign are modulated by terms that originate in diffractive propagation and in nonlocal interaction of the field with itself.
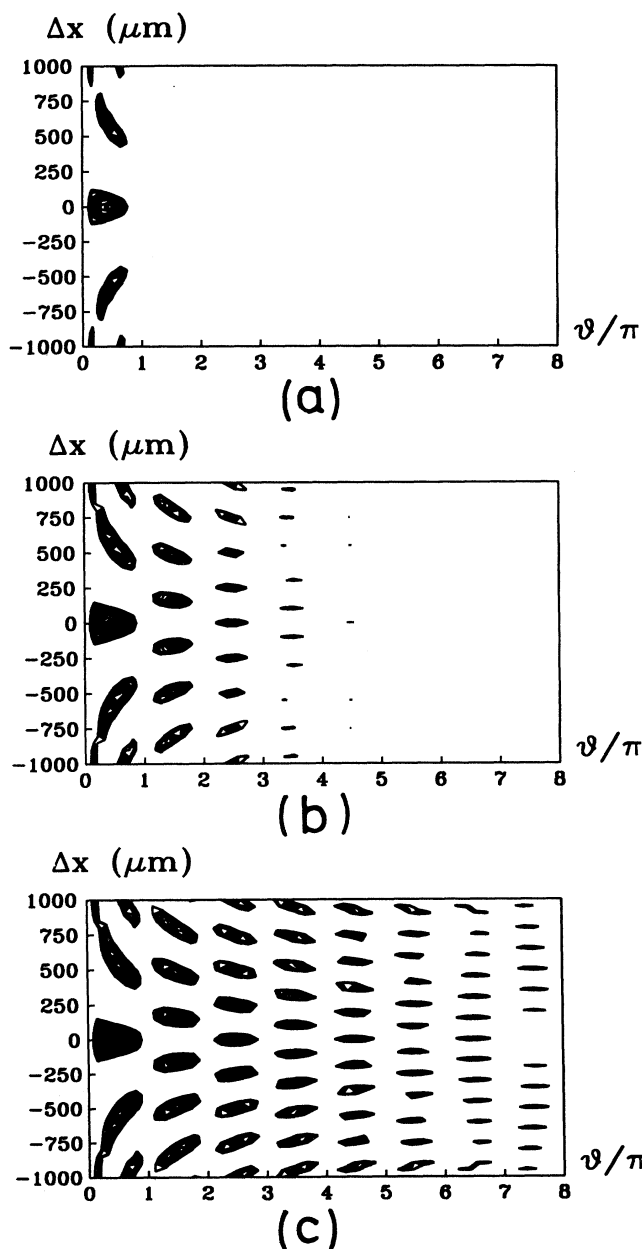

FIG. 2. Level lines of the quantity $\tau\lambda > 0$ in the $(\theta, \Delta x)$ plane. $\beta = 0.8$ cm^2/mW, $I_0 = 5$ mW/cm^2, and $l = 23$ cm (focusing case). (a) $\sigma = 3$. (b) $\sigma = 10$. (c) $\sigma = 30$.
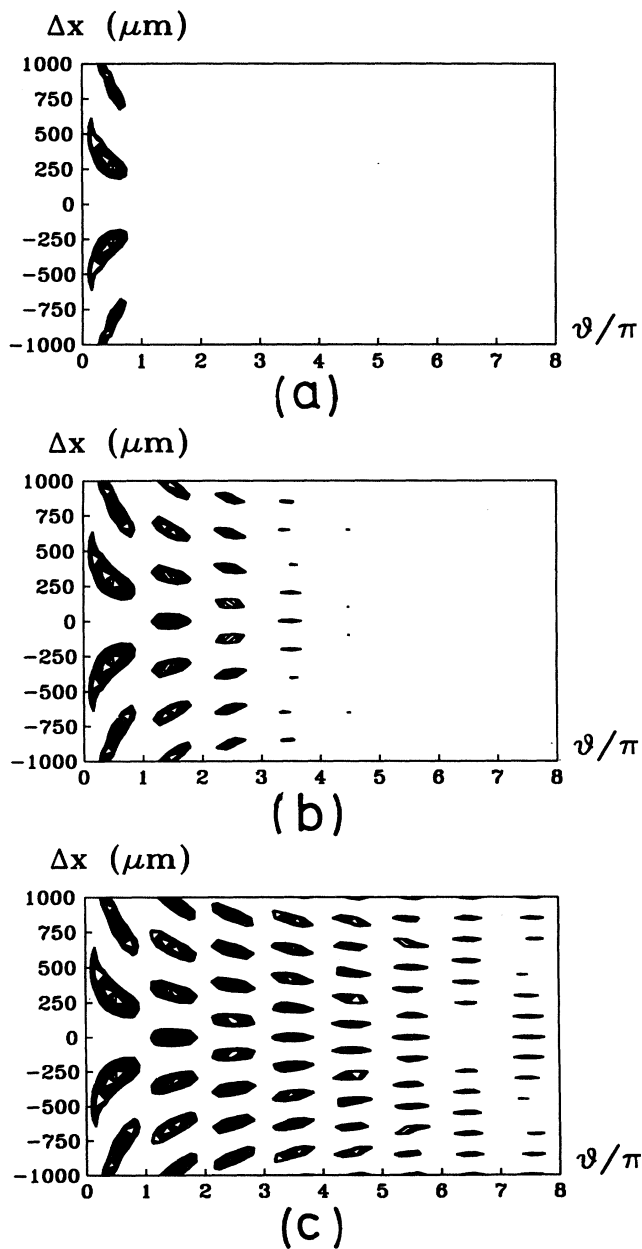

FIG. 3. Level lines of the quantity $\tau\lambda > 0$ in the $(\theta, \Delta x)$ plane. $\beta = -0.8$ cm^2/mW, $I_0 = 5$ mW/cm^2, and $l = 23$ cm (defocusing case). (a) $\sigma = 3$. (b) $\sigma = 10$. (c) $\sigma = 30$.

For fixed values of β, I_0, σ, and l, in plane $(\theta, \Delta x)$ we plot the level lines corresponding to $\tau\lambda > 0$. The result is shown in Fig. 2 for $\beta > 0$ (focusing medium) and in Fig. 3 for $\beta < 0$ (defocusing medium) for three different values of σ. Each island in these plots corresponds to an instability region. As can be expected, for increasing diffusion length (i.e., for decreasing σ) a suppression of the modes with high θ is observed both for the focusing and defocusing cases. Along line $\Delta x = 0$ the results of Ref. [3] are found; i.e., the first unstable mode corresponds to $\theta \simeq \pi/2$ for $\beta > 0$ and to $\theta \simeq \frac{3}{2}\pi$ for $\beta < 0$.

In Figs. 4 and 5 we plot the level lines corresponding to $\tau\Omega > 0$ in the plane $(\theta, \Delta x)$. Since the quantity $\tau\Omega$ is an odd function of Δx, it is clear that for any positive peak in Figs. 4 and 5 there is a corresponding negative peak at the symmetrical position with respect to the $\Delta x = 0$ axis. The negative part of the plot is not shown here for clarity. Along line $\Delta x = 0$ it is found that here $\Omega = 0$, this meaning that in the absence of the transport term only stationary patterns can bifurcate [3].

Moving along the Δx direction, the plots shown in Figs. 2 and 3 predict two fundamentally different kinds of behavior for the system. First, it is possible that the system suddenly jumps from one island of instability to another one centered at a different value of θ. Second, when the system is on a well defined island, a variation in Δx can result in a slow, continuous variation of θ. As for the time behavior of the patterns, it is clear from Figs. 4 and 5 that a frequency $\Omega \neq 0$ appears, resulting in the bifurcation of a drifting roll pattern, as soon as the system moves away from the very center of an island (the point of that island corresponding to the maximum value of $\tau\lambda$). It is worth noting that, while in the case of a focusing medium there is always a region of maximum instability for $\Delta x = 0$, in the case of a defocusing medium this is no longer true. In other words, the instability threshold for a defocusing medium is lower for $\Delta x \neq 0$ than for $\Delta x = 0$. For this reason it seems appropriate to us to talk of transport-induced instability in this last case.
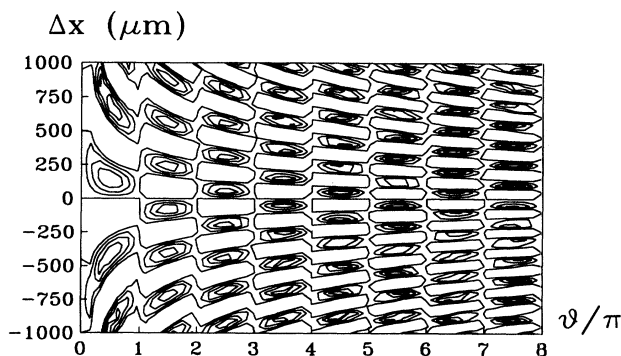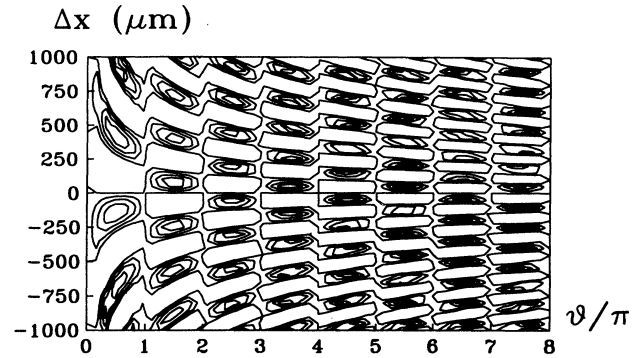
$$\Delta x \;\; (\mu\text{m})$$

FIG. 4. Level lines of the quantity $\tau\Omega > 0$ in the $(\theta, \Delta x)$ plane. $\beta = 0.8$ cm^2/mW, $I_0 = 5$ mW/cm^2, and $l = 23$ cm (focusing case).

$$\Delta x \;\; (\mu\text{m})$$

FIG. 5. Level lines of the quantity $\tau\Omega > 0$ in the $(\theta, \Delta x)$ plane. $\beta = -0.8$ cm^2/mW, $I_0 = 5$ mW/cm^2, and $l = 23$ cm (defocusing case).

V. EXPERIMENTAL RESULTS AND COMPARISON WITH THE MODEL

All experimental observations were performed for fixed values of the parameters $l = 23$ cm (free propagation length in the feedback loop), $V_0 = 7.5$-V rms and $f_0 = 15$ kHz (amplitude and frequency of the sinusoidal voltage applied to the LCLV). The slit located in plane z_i measures 9.9×0.18 mm^2. Since for the values of optical wavelength λ and free propagation l used we expect that the scale of the unstable modes be of the order of hundreds of μm, this slit should be adequate in order to render the system nearly one dimensional. As control parameters we used the intensity I_0 of the light beam impinging on the front side of the LCLV (a fraction $\simeq 0.45$ of this light is fed back to the rear side of the LCLV) and the translation Δx introduced in the feedback loop.

We indeed observed that the structures formed inside the active window delimited by the slit are strongly dependent on the value of Δx. Due to the one-dimensional nature of the setup, the patterns are always, at least approximately, rolls oriented orthogonally with respect to the long side of the slit. By varying the value of Δx, we observed variations in the amplitude of these rolls. In particular, it is possible to pass from values of Δx for which the amplitude of the rolls is zero (uniform regime), to others for which the intensity modulation of the roll pattern can be of the order of unity.

Furthermore the value of Δx determines the wavelength Λ (and hence the wave number $q = 2\pi/\Lambda$) of the observed structure. In some regions the variations of Λ vs Δx appear to be smooth, while in others it is possible to notice the existence of discontinuous jumps of the value of Λ from one band to another. The rolls can be either stationary or traveling at a constant speed along the x direction. Since these structures are periodic in space, a time frequency Ω, whose value depends on Δx, is associated with their uniform drift motion. All these observations are in qualitative agreement with the prediction of
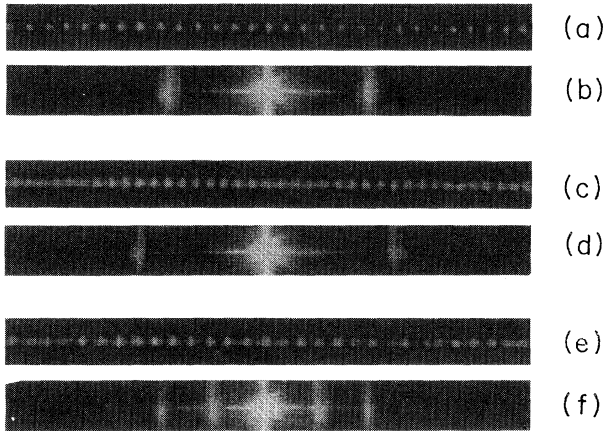
FIG. 6 Near field [(a),(c), and (e)] and corresponding far field [(b), (d), and (f)] images of the signal. $I_0=9.4$ mW/cm^2. $\Delta x=30$ μm [(a) and (b)], 110 μm [(c) and (d)], and 150 μm [(e) and (f)]. Note the presence of a strong second harmonic component in (e) and (f).

the model discussed in Sec. II.

The linear stability analysis predicts also a linear dependence of the drift frequency Ω vs the input intensity I_0. In order to check the validity of this prediction, we performed a series of experimental observations of the dependence of Ω vs I_0, for fixed values of Δx. We verified that Ω indeed depends on I_0, but not in a linear way over all the range of I_0 we investigated. Indeed, it is to be expected that there are some discrepancies between predictions based on the linear stability analysis and the results of experiments for those values of the parameters driving the system far above threshold. This is just what happens when increasing the value of I_0 too much. In this regime, we also observed some phenomena that are qualitatively different from the simple ones predicted by the linearized model. In particular, it is possible to observe irregular time fluctuations of the spatial phase of the roll pattern, and also the coexistence of structures belonging to different q bands.
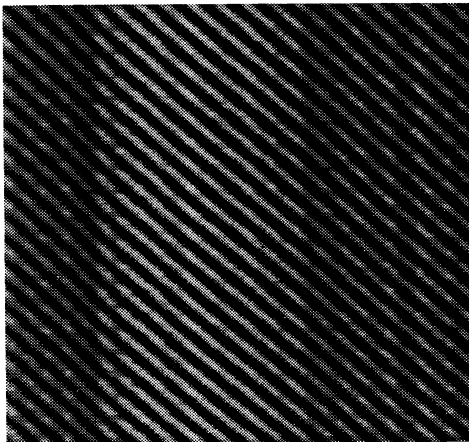

FIG. 7. Space (horizontal)-time (vertical) evolution of the near field signal. $I_0=6$ mW/cm^2; $\Delta x=150$ μm.

We measured the spatial frequency q and the temporal drift frequency Ω of the roll patterns vs the displacement Δx of the feedback fields for three different values of the input intensity I_0, namely, $I_0=3$, 6, and 9.4 mW/cm^2. The values of the spatial frequency q were deduced from measurements performed in the far field of the signal, corresponding to the Fourier spectrum of the signal itself. Typical examples of the near field of the signal and of the corresponding far field are shown in Fig. 6. In order to measure q we isolated the central line of the far field, and acquired for each value of Δx a set of 200 samples of this line. We then calculated the average line in order to
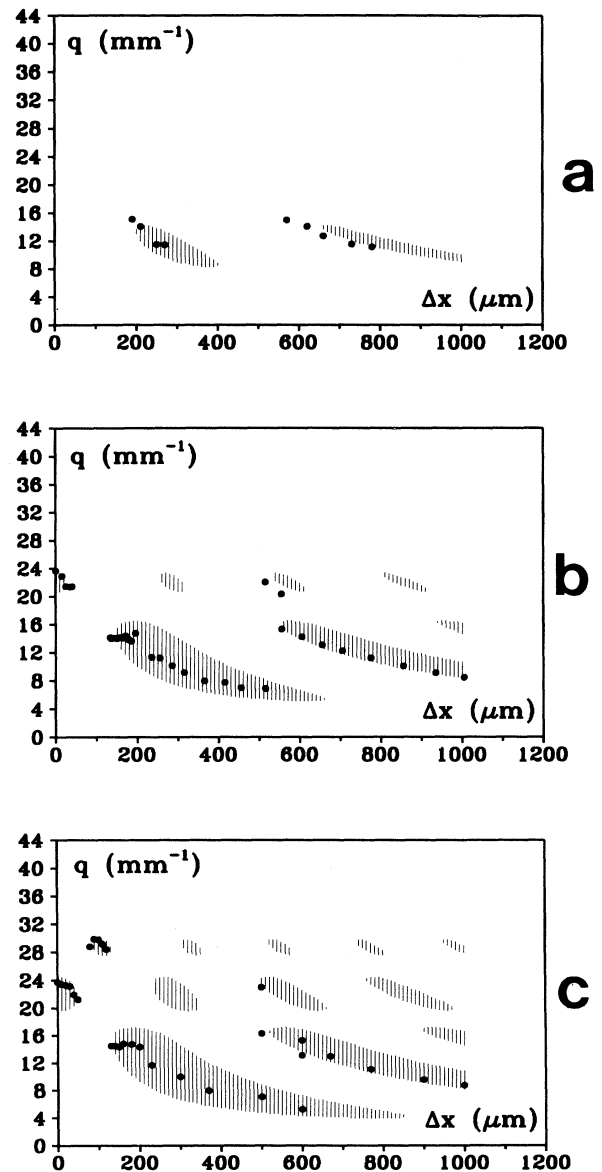

FIG. 8. Wave number q of the unstable mode(s) vs Δx. $I_0=3$ (a), 6 (b), and 9.4 (c) mW/cm^2. Filled dots: experimental points. Shadowed regions: simulations from Eq. (9a) with $\tau=250$ ms, $\beta=-0.8$ cm^2/mW, and $\sigma=3$.

reduce the signal to noise ratio, and finally evaluated the values of q from this average line.

The temporal drift frequency of the rolls was measured starting from the acquisition of 200 samples of the central line in the near field for each value of Δx. The samples are separated in time by 0.08. The succession of the 200 lines forms an image representing the space time evolution of the central line of the near field signal. A typical example of one of these images is shown in Fig. 7. The temporal drift frequency of the rolls is derived from these space time plots by counting the number of maxima crossing a fixed coordinate in the unit of time. The re-

sults of the measurements of q and Ω vs Δx are shown in Figs. 8 and 9.

Let us concentrate first on the plot of q vs Δx. It is seen here that, for low values of input intensity ($I_0 = 3$ mW/cm^2) the system is on the uniform solution for $\Delta x = 0$, while it displays a transport-induced instability leading to the roll solution for $\Delta x \neq 0$. For higher values of I_0 ($I_0 = 6$, and 9.4 mW/cm^2) the roll solution is already above threshold for $\Delta x = 0$. For increasing Δx it is possible to observe either a continuous variation of the q value, or a series of sudden jumps of q from one band to another. The number of the bands influenced by the instability increases for increasing I_0, and in some cases the coexistence of two bands can be observed.

Consider now the plots of Ω vs Δx. For $I_0 = 3$ mW/cm^2 The roll structure results to be always stationary. At higher value of I_0, the rolls can drift with a frequency whose magnitude and sign (corresponding to the direction of the motion along x) depends on Δx. For very high values of I_0 and Δx, finally, we have observed some
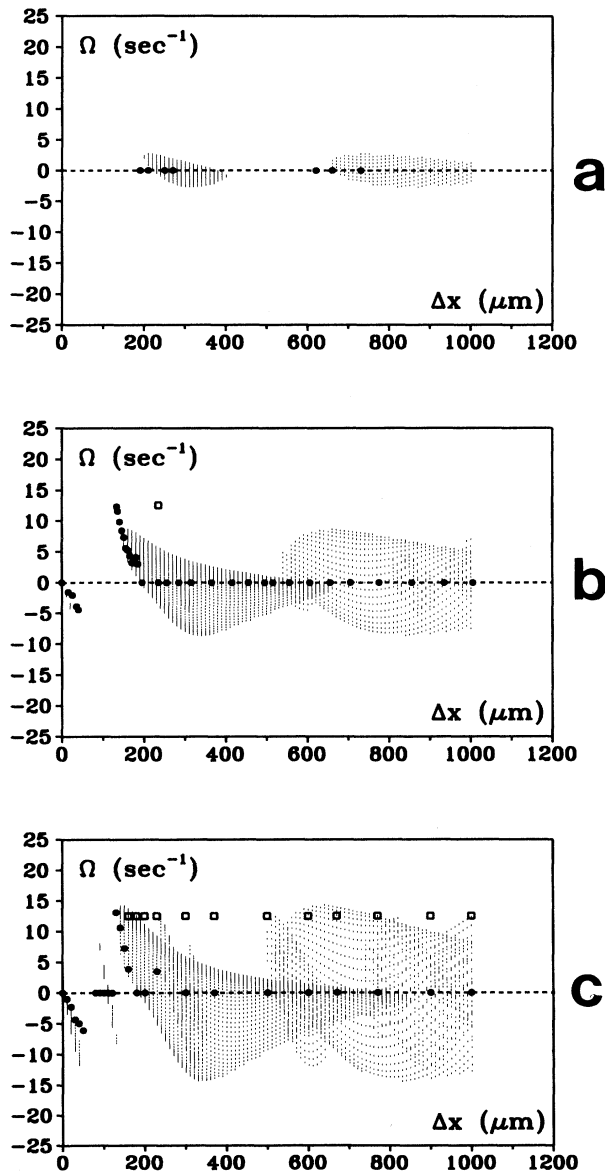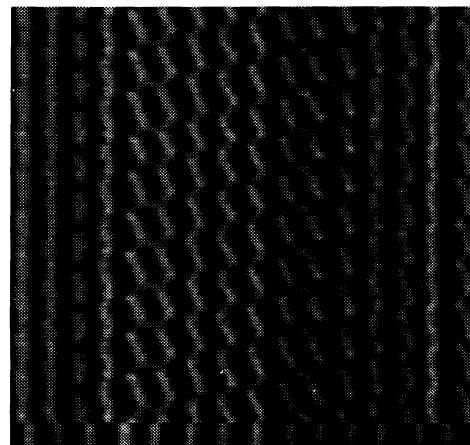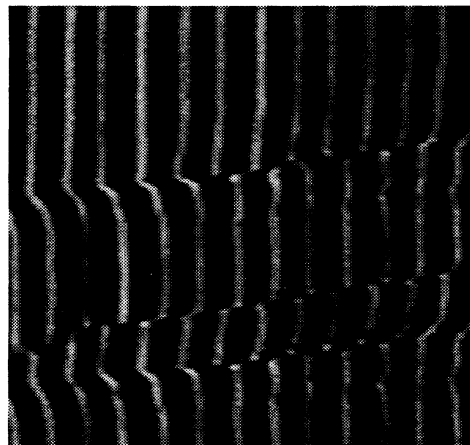

FIG. 9. Temporal frequency Ω of the unstable mode(s) vs Δx. $I_0 = 3$ (a), 6 (b), and 9.4 (c) mW/cm^2. Filled dots: experimental points. Shadowed regions: simulations from Eq. (9a) with $\tau = 250$ ms, $\beta = -0.8$ cm^2/mW, and $\sigma = 3$. The empty squares indicate phase fluctuation regimes.

FIG. 10. Space (horizontal)-time (vertical) evolution of the near field signal in the phase fluctuation regime. $I_0 = 9.4$ mW/cm^2. $\Delta x = 235$ μm (a) and 300 μm (b).
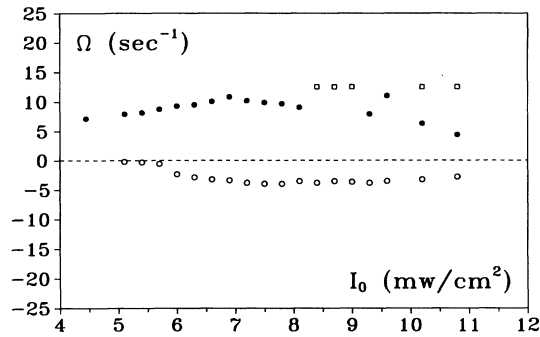
FIG. 11. Temporal frequency Ω of the unstable mode(s) vs I_0. Empty dots: $\Delta x = 30$ μm. Full dots: $\Delta x = 150$ μm. The empty squares indicates phase fluctuation regimes for $\Delta x = 150$ μm.

response time τ, the nonlinearity parameter β, and the ratio σ of diffusive to diffractive square lengths. We find the best agreement between theory and experimental data for the following values of the parameters: $\tau = 250$ ms; $\beta = -0.8$ cm^2/mW; and $\sigma = 3$, corresponding to $l_d \simeq 80$ μm. These values are in fair agreement with the typical characteristic parameters of the LCLV [16]. The results derived from the numerical simulations of the model are represented as shadowed regions in Figs. 8 and 9. It is seen here that results from theory and experiments fit well for values of I_0 and Δx that are not too high. Since theoretical predictions come from a linear stability analysis, some discrepancies are to be expected for those values of I_0 which drive the system far above threshold. Furthermore, for high values of Δx it is possible that the limited longitudinal size of the system introduces some deviations from the ideal, infinite size model.

qualitatively different phenomena from those predicted by the linear stability analysis of the model. In fact, there are situations in which the rolls are neither stationary nor drifting, but rather display phase fluctuations that can be either regular or irregular in time. Space time plots relative to two of these situations are shown in Fig. 10.

Another series of measurements has been devoted to the investigation of the dependence of the roll drift frequency Ω vs the input intensity I_0. These measurements were done for two different values of Δx, namely $\Delta x = 30$ and 150 μm, corresponding, respectively, to situations in which Ω is negative and positive. The experimental results reported in Fig. 11 show that the theoretical prediction of a linear dependence of Ω vs I_0 is approximately verified only for values of I_0 that are not too high.

For the measurements of q vs Δx an Ω vs Δx discussed above we have performed a quantitative comparison between the experimental results and the predictions of the model. This was done by using Eqs. (9a) and (9b) of Sec. III. For fixed l, the free parameters are the LCLV

VI. CONCLUSIONS

We have theoretically analyzed and experimentally demonstrated the onset of a pattern forming drifting instability in an optical system in which nonlocality is introduced in the feedback loop by means of a translation. The main prediction derived from the model, namely the existence of a reduced threshold for pattern formation in defocusing media when nonlocality is introduced, is experimentally confirmed.

When the system is driven far above threshold, phenomena of phases fluctuations and of locking at zero temporal frequency of the patterns are observed. These phenomena, that we hypothesize as due to the onset of secondary bifurcations, are the subject of a present investigation.

ACKNOWLEDGMENT

[1] M. C. Cross and P. C. Hohenberg, Rev. Mod. Phys. **65**, 851 (1993).

[2] See, e.g., *Nonlinear Dynamics and Spatial Complexity in Optical Physics*, edited by R. G. Harrison and J. S. Uppal (SUSSP, Edinburgh, 1993); F. T. Arrechi, Nuovo Cimento A **107**, 1111 (1994); *Chaos, Solitons Fractals* **4**, Special issues 8 and 9 (1994).

[3] G. D'Alessandro and W. J. Firth, Phys. Rev. Lett. **66**, 2597 (1990); G. D'Alessandro and W. J. Firth, Phys. Rev. A **46**, 537 (1992).

[4] S. A. Akhmanov, M. A. Vorontsov, and V. Yu. Ivanov, Pis'ma Zh. Eksp. Teor. Fiz. **47**, 111 (1988) [JETP Lett. **47**, 707 (1988)]; S. A. Akhmanov, M. A. Vorontsov, and V. Yu. Ivanov, A. V. Larichev, and N. I. Zheleznykh, J. Opt. Soc. Am. B **9**, 78 (1992).

[5] E. Pampaloni, S. Residori, and F. T. Arecchi, Europhys.

Lett. **24**, 647 (1993); E. Pampaloni, P. L. Ramazza, S. Residori, and F. T. Arecchi, Phys. Rev. Lett. **74**, 258 (1995).

[6] M. Haeltermann and G. Vitrant, J. Opt. Soc. Am. B **9**, 1563 (1992).

[7] P. La Penna and G. Giusfredi, Phys. Rev. A **48**, 2299 (1993).

[8] G. Grynberg, Opt. Commun. **109**, 483 (1994).

[9] A. Petrossian, L. Dambly, and G. Grynberg, Europhys. Lett. **29**, 209 (1995).

[10] R. W. Walden, P. Kolodner, A. Passner, and C. M. Surko, Phys. Rev. Lett. **55**, 496 (1985).

[11] I. Mutabazi, J. J. Hagseth, C. D. Andereck, and J. E. Wesfried, Phys. Rev. A **38**, 4752 (1988).

[12] I. Rehberg, S. Rasenat, and V. Steinberg, Phys. Rev. Lett. **62**, 756 (1989).

[13] S. Douady, S. Fauve, and O. Thual, Europhys. Lett. **10**, 309 (1989).

[14] M. Rabaud, S. Michellaud, and Y. Couder, Phys. Rev. Lett. **64**, 184 (1990).

[15] S. Fauve, S. Douady, and O. Thual, J. Phys. (France) II **1**, 311 (1991).

[16] M. A. Vorontsov, M. E. Kirakosyan, and A. V. Larichev, Kuant. Elektron. (Moscow) **18**, 117 (1991) [Sov. J. Quantum Electron. **21**, 105 (1991)].
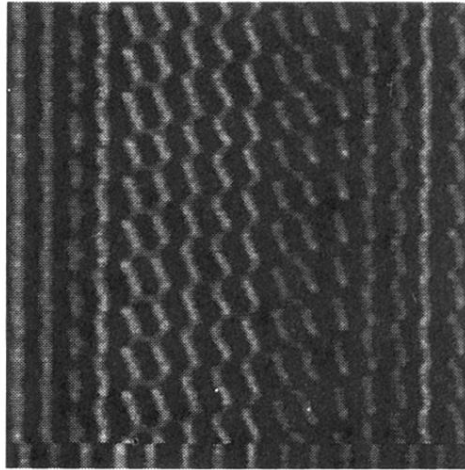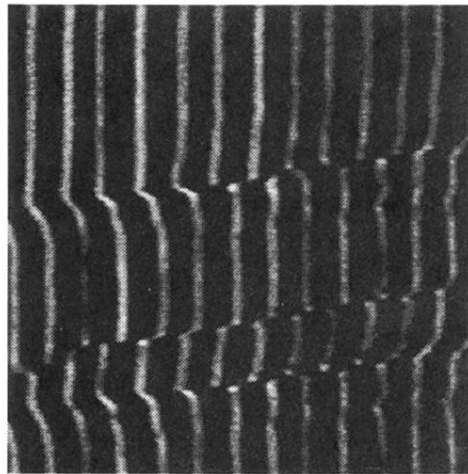
FIG. 10. Space (horizontal)-time (vertical) evolution of the near field signal in the phase fluctuation regime. $I_0 = 9.4$ mW/cm.^{2} $\Delta x = 235 \ \mu$m (a) and $300 \ \mu$m (b).
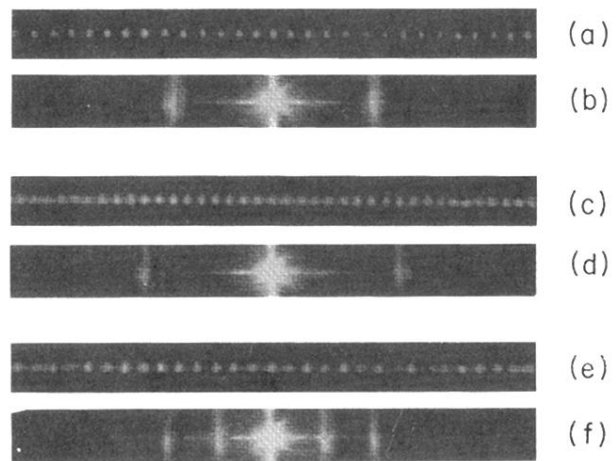
FIG. 6 Near field [(a),(c), and (e)] and corresponding far field [(b), (d), and (f)] images of the signal. $I_0 = 9.4$ mW/cm^2. $\Delta x = 30$ μm [(a) and (b)], 110 μm [(c) and (d)], and 150 μm [(e) and (f)]. Note the presence of a strong second harmonic component in (e) and (f).
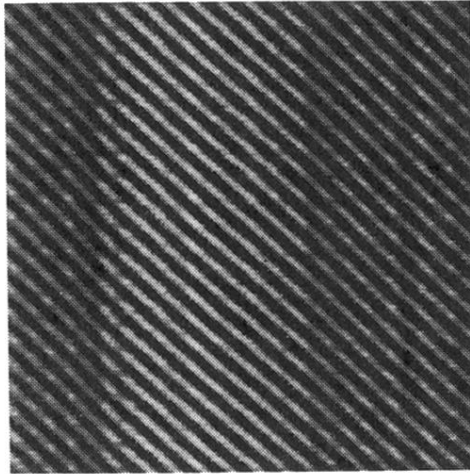
FIG. 7. Space (horizontal)-time (vertical) evolution of the near field signal. $I_0 = 6$ mW/cm^2; $\Delta x = 150$ μm.